IEEE Access
Multidisciplinary | Rapid Review | Open Access Journal

Received 31 October 2022, accepted 16 November 2022, date of publication 18 November 2022,
date of current version 23 November 2022.

*Digital Object Identifier 10.1109/ACCESS.2022.3223352*

RESEARCH ARTICLE

# Droop Controlled Microgrid With DSTATCOM for Reactive Power Compensation and Power Quality Improvement

**KUANG-HSIUNG TAN[1], (Member, IEEE), MENG-YANG LI[2], AND XIANG-YU WENG[2]**
[1]Department of Electrical and Electronic Engineering, Chung Cheng Institute of Technology, National Defense University, Taoyuan 335, Taiwan
[2]Department of Electrical Engineering, National Central University, Chungli, Taoyuan 320, Taiwan

Corresponding author: Kuang-Hsiung Tan (s913115@gmail.com)

This work was supported by the Ministry of Science and Technology of Taiwan under Grant MOST 111-3116-F-008-003.

**ABSTRACT** A droop controlled microgrid with distribution static compensator (DSTATCOM) is developed to improve the power quality in this study. Due to the reactive power/voltage $Q$-$V$ droop characteristic and the existence of the unbalanced, linear inductive and nonlinear loads, the power quality problems, including the voltage drop, unbalanced currents, lagging power factor (PF) and current harmonics, are very serious in the islanded microgrid. Moreover, owing to the instantaneous power following into or out of the DC-link capacitor of the DSTATCOM under load variation, the performance of the DSTATCOM for power quality improvement is seriously degenerated. Hence, to effectively improve the power quality of the droop controlled microgrid and the transient response of the DC-link voltage of the DSTATCOM under load variation, an online trained polynomial petri fuzzy neural network (PPFNN) controller is firstly proposed as the DC-link voltage controller to supersede the conventional proportional-integral (PI) controller in the DSTATCOM. The network structure and the online learning strategy of the proposed PPFNN are detailedly derived. Finally, the effectiveness of the DSTATCOM using the proposed PPFNN controller to improve the unbalanced currents, the total harmonic distortion (THD) reduction of the current and to compensate the reactive power for the voltage support and PF correction in the droop controlled microgrid is certified.

**INDEX TERMS** Microgrid, droop control, DSTATCOM, power quality, intelligent control, polynomial neural network.

## I. INTRODUCTION

In the past decade, owing to the penetration of the electric vehicle, charging station, storage system and renewable energy-based distributed generator (DG), the conventional power system has been changed. A novel conception of power system named as microgrid to combine the different DGs with local loads through the power electronic converter has been arisen [1], [2], [3], [4]. The microgrid can perform in grid-connected mode and islanding mode [2], [3]. However, the power quality and system reliability of the microgrid aren't necessarily ensured owing to the intermittent characteristics of the different DGs [5]. Moreover, in terms of control algorithm, the droop control strategy is extensively implemented in the microgrid [6]. The droop control strategies are composed of the $P$-$\omega$ and $Q$-$V$ droop controls. In accordance with the characteristics of the droop controls, the DGs in the islanding microgrid will reduce the voltage amplitude and system frequency to share the reactive power and active power for balancing the supply and demand [4]. Nevertheless, the frequency control and stability of the microgrid need to be considered. Much literature [7], [8], [9] had been researched for power quality improvement with regard to the frequency control and stability of the microgrid. In [7], a hybrid power generating system equipped with a supercapacitor was proposed to eliminate the ripple in the power system. A dual-stage fractional order PID controller for enhancing the frequency control of the islanding and interconnected multi-$\mu$grids was proposed in [8]. In [9], a novel fuzzy tilt integral derivative with a filter plus double

The associate editor coordinating the review of this manuscript and approving it for publication was Yu-Da Lin.

integral control method had been proposed to eliminate the frequency variations in a hybrid system. On the other hand, one of the serious power quality issues in the droop controlled microgrid operated in islanding mode is voltage drop [5]. Furthermore, the traditional droop controls also suffer several drawbacks, such as the slow dynamic response, poor harmonic compensation capability, the lack of decoupling capability and so on [10], [11]. In addition, owing to the existence of the unbalanced, linear inductive and nonlinear loads, the unbalanced currents, lagging power factor (PF) and current harmonic components may occur in the microgrid resulted in the deteriorated power quality [10], [11], [12]. Hence, the way to improve the power quality and compensate the reactive power for the voltage support in the droop controlled microgrid operated in islanding mode is essential [13], [14].

Distribution static compensator (DSTATCOM) is one of effectual methods to overcome the power quality issues and voltage support in the microgrid [15], [16], [17]. The DSTATCOM can be categorized into two types: 1) synchronous reference frame (SRF) theory and 2) instantaneous reactive power (IRP) theory [18], [19], [20]. Because the SRF theory is mainly based on the $dq0$ synchronous reference frame and adopts the phase-locked loop (PLL), the SRF theory can be denominated as $dq$ theory. Nevertheless, on account of the long computation time by using PLL and the generation of the undesirable second order harmonics [20], the efficiency of the SRF theory for power quality improvement should be deliberated. On the other hand, the IRP theory is widely adopted in the DSTATCOM because it is performed in $\alpha\beta$ stationary reference frame without using the PLL for transferring to $dq0$ axes [20]. The computation time of the IRP theory can be much reduced. Many researches adopted the DSTATCOM for power quality improvement have been investigated [5], [12], [21]. A coordinated control of the DG and DSTATCOM in a microgrid is proposed to improve the power quality [5]. An online reference control strategy for the DSTATCOM using the reinforcement learning algorithm is provided in [12]. In [21], a control scheme of STATCOM is proposed for doubly fed induction generator based wind farm to minimize the capacity of centralized reactive power compensation. In general, an energy buffer element, namely the DC-link capacitor, is necessarily equipped at the DC side of the DSTATCOM. The main functions of the DC-link capacitor are to maintain the constant DC voltage and to generate the mitigation or injection current to the source current for the normal operation [22]. Nevertheless, since the instantaneous power will follow into or out of the DC-link capacitor of the DSTATCOM at the moment of the load change, the transient responses of the system currents and DC-link voltage fluctuate seriously resulted in the deteriorated power quality improvement. Consequently, it is important for the DSTATCOM to maintain the constant DC-link voltage under load variation [23], [24].

Lately, fuzzy neural network (FNN) has been extensively adopted in different areas. The FNN is to integrate the fuzzy logic into artificial neural network (NN) [25], [26], [27], [28]. The operating principle of the fuzzy logic theory is to utilize the ''IF–THEN'' rules made by expert's experience for control system. And the fuzzy logic theory doesn't need the accurate mathematical model for the control process [26]. Moreover, on account of the self-learning capability and adaptability, the NN can deal with the prediction and estimation of time series problem [28]. Hence, the FNN can effectively cope with the nonlinear, complicated and time-varying systems [26]. In [28], an active power filter using short-term memory FNN was proposed to reduce the current harmonics. In [29], the FNN was adopted for stock prediction via distributed parallelism. Furthermore, petri net (PN) was developed for the investigation of communication with automata [3]. Due to the mathematical modeling and analytical capabilities, PN is an effective solution to model the discrete event systems and to describe the concurrent and asynchronous structure of the services [30], [31], [32]. Some literature using PN has been proposed. In [33], PN is proposed for treatment and fault detection in automated manufacturing system. On the other hand, the polynomial neural network (PNN) combines the polynomial theory with NN. The main purpose of polynomial theory is to adopt the predictive polynomials for the complicated dynamic system [34]. Thus, the PNN owns the capability in reflecting high-order nonlinear relations between the input and output variables, and the ability to concisely express any functions on a finite sample dataset based on its structure [35], [36], [37]. In this study, according to the above capabilities of FNN, PN and PNN, an online trained polynomial petri fuzzy neural network (PPFNN) controller is firstly proposed.

A droop controlled microgrid with the IRP theory based-DSTATCOM is developed in this study. To solve the power quality issues of the droop controlled microgrid, including the voltage drop, unbalanced currents, lagging PF and current harmonics, and to improve the transient response of DC-link voltage of the DSTATCOM under the sudden load variations, an online trained PPFNN is firstly proposed as the DC-link voltage controller to supersede the conventional proportional-integral (PI) controller in the DSTATCOM. The operating principles of the droop controlled microgrid and the DSTATCOM using the IRP theory are detailedly described in Section II. The network structure and online learning strategy of the proposed PPFNN controller are derived in Section III. Then, the feasibility and effectiveness of the DSTATCOM using the proposed PPFNN controller to improve the unbalanced currents, the total harmonic distortion (THD) reduction of the current and to compensate the reactive power for the voltage support and PF correction in the droop controlled microgrid are certified in Section IV. Finally, some conclusions will be depicted in Section V.

## II. DROOP CONTROLLED MICROGRID WITH DSTATCOM

In this study, the architecture of the droop controlled microgrid with the DSTATCOM and various loads is represented in Fig. 1. The microgrid is composed of the battery energy storage system (BESS), DSTATCOM, unbalanced load,

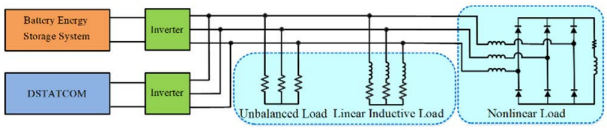


**FIGURE 1.** Architecture of droop controlled microgrid with DSTATCOM and various loads.

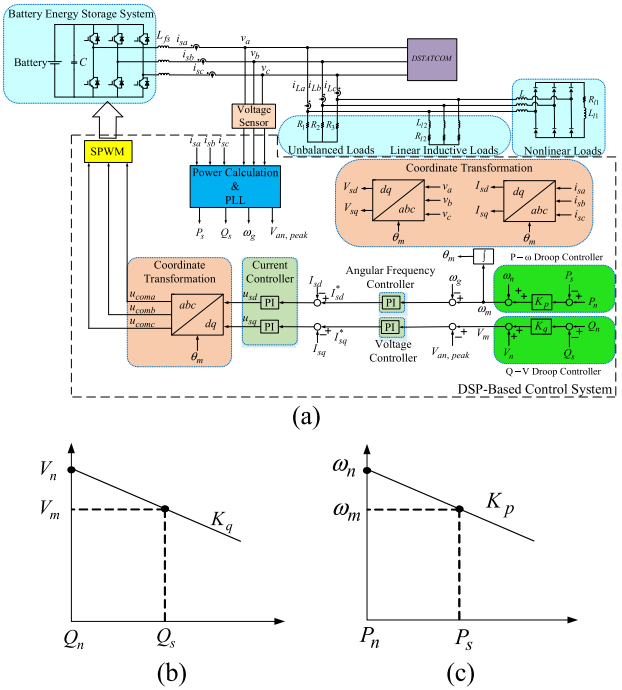


**FIGURE 2.** Block diagram of storage system. (a) Control block of storage system using droop control. (b) $Q-V$ droop control. (c) $P-\omega$ droop control.

linear inductive load and the nonlinear load. The various loads result in the deteriorated power quality, including the three-phase unbalanced currents, lagging PF and the current harmonics. Moreover, the droop controlled microgrid is operated in islanding mode. The operating principles of the storage system and the DSTATCOM are detailedly depicted as follows:

### A. STORAGE SYSTEM USING DROOP CONTROL

The block diagram of the storage system is illustrated in Fig. 2. The control block of the storage system using the droop control is shown in Fig. 2(a). Firstly, the $dq$-axis voltages and currents $V_{sd}$, $V_{sq}$, $I_{sd}$ and $I_{sq}$ are acquired for the block of power calculation and PLL by the three-phase system voltages $v_a$, $v_b$, $v_c$ of the microgrid and the three-phase output currents $i_{sa}$, $i_{sb}$, $i_{sc}$ of the storage system using the $abc/dq$ coordinate transformation. Then, the peak value of the phase voltage $V_{an,peak}$ and the angular frequency $\omega_g$ of the microgrid system, the active power $P_s$ and reactive power $Q_s$ of the storage system are computed for the droop controls. The characteristics of the $Q$-$V$ and $P$-$\omega$ droop controls adopted in the storage system are represented in Figs. 2(b) and 2(c) and described as follows [4]:

$$V_m = V_n + K_q(Q_n - Q_s) \tag{1}$$

$$\omega_m = \omega_n + K_p(P_n - P_s) \tag{2}$$

where $Q_n$ and $P_n$ are the reference values of the reactive and active powers at no load, which are designed to be 0 Var and 0 W, respectively; $K_q$ and $K_p$ are the droop coefficients, which are set to be $1/20$ V/Var and $1.3/600$ (rad/s)/W respectively; $V_n$ and $\omega_n$ are the reference values of the phase voltage and angular frequency at no load, which are designed to be 89.8 V and 377 rad/s respectively; $V_m$ and $\omega_m$ are the amplitude of phase voltage and the output angular frequency. In accordance with Eq. (2), the electric angle $\theta_m$ is calculated by the output angular frequency $\omega_m$ via the integral operation for the coordinate transformation as shown in Fig. 2(a). Moreover, the angular frequency error $\omega_m - \omega_g$ and the voltage error $V_m - V_{an,peak}$ are sent to the PI controllers to obtain the $dq$-axis current commands $I^*_{sd}$ and $I^*_{sq}$. Finally, the current commands $u_{coma}$, $u_{comb}$, $u_{comc}$ are computed through the $dq/abc$ coordinate transformation for the sinusoidal pulse width modulation (SPWM) switching signals.

### B. DSTATCOM USING IRP THEORY

The control block of DSTATCOM using the IRP theory to improve the power quality is provided in Fig. 3. Firstly, the three-phase load currents $i_{La}$, $i_{Lb}$, $i_{Lc}$ and the system voltages $v_a$, $v_b$, $v_c$ of the microgrid are detected and transferred to the $\alpha\beta 0$ stationary reference frame in the following for the calculation of instantaneous active and reactive powers [20]:

$$\begin{bmatrix} i_{L\alpha} \\ i_{L\beta} \\ i_{L0} \end{bmatrix} = \frac{2}{3}\begin{bmatrix} 1 & -\frac{1}{2} & -\frac{1}{2} \\ 0 & -\frac{\sqrt{3}}{2} & \frac{\sqrt{3}}{2} \\ \frac{1}{2} & \frac{1}{2} & \frac{1}{2} \end{bmatrix}\begin{bmatrix} i_{La} \\ i_{Lb} \\ i_{Lc} \end{bmatrix} \tag{3}$$

$$\begin{bmatrix} v_\alpha \\ v_\beta \\ v_0 \end{bmatrix} = \frac{2}{3}\begin{bmatrix} 1 & -\frac{1}{2} & -\frac{1}{2} \\ 0 & -\frac{\sqrt{3}}{2} & \frac{\sqrt{3}}{2} \\ \frac{1}{2} & \frac{1}{2} & \frac{1}{2} \end{bmatrix}\begin{bmatrix} v_a \\ v_b \\ v_c \end{bmatrix} \tag{4}$$

where $i_{L\alpha}$, $i_{L\beta}$ and $i_{L0}$ are the $\alpha$, $\beta$ and zero axis currents of loads; $v_\alpha$, $v_\beta$ and $v_0$ are the $\alpha$, $\beta$ and zero axis voltages of microgrid. Thereupon, the instantaneous active power $P_L$ and reactive power $Q_L$ of the loads are obtained as follows [19]:

$$\begin{bmatrix} P_L \\ Q_L \end{bmatrix} = \begin{bmatrix} v_\alpha & v_\beta \\ -v_\beta & v_\alpha \end{bmatrix}\begin{bmatrix} i_{L\alpha} \\ i_{L\beta} \end{bmatrix} \tag{5}$$

Moreover, the instantaneous active power $P_L$ and reactive power $Q_L$ are composed of the average (dc) and alternating (ac) components in the following:

$$P_L = \bar{P}_L + \tilde{P}_L \tag{6}$$

$$Q_L = \bar{Q}_L + \tilde{Q}_L \tag{7}$$

where $\bar{P}_L$ and $\bar{Q}_L$ are the average components and $\tilde{P}_L$ and $\tilde{Q}_L$ are the alternating components of the instantaneous active power and reactive power. The average components depict the product of the fundamentals of the load current and system voltage. The alternating components express the power

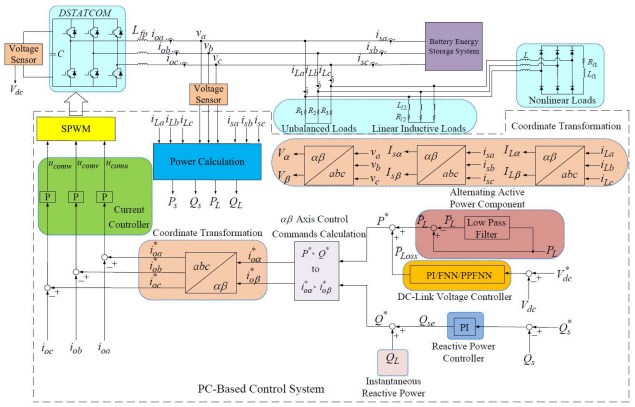


**FIGURE 3.** Control block of DSTATCOM.

related to the product of the harmonic components of the load current and system voltage. In Fig. 3, the average active power component $\bar{P}_L$ is obtained through a low pass filter. The alternating active power component $\tilde{P}_L$ is acquired by deducting the average active power component $\bar{P}_L$ from the instantaneous active power $P_L$. Furthermore, owing to the load variation, filter loss and switching loss, the instantaneous power follows into or out of the DC-link capacitor of the DSTATCOM resulted in the fluctuating DC-link voltage and poor power quality improvement. Consequently, the DC-link voltage command $V_{dc}^*$ is compared with the DC-link voltage $V_{dc}$ for the generation of the voltage error, which is sent to DC-link voltage controllers, namely PI, FNN and the proposed PPFNN, to generate the power loss $P_{loss}$ for maintaining the constant DC-link voltage and enhancing the power quality improvement under load variation. The active power command $P^*$ is obtained by adding the power loss $P_{loss}$ to the alternating active power component $\tilde{P}_L$. In addition, the reactive power command $Q_s^*$ of the storage system is compared with the reactive power $Q_s$. Afterward, the reactive power error is sent to the PI controller to generate the reactive power correction $Q_{se}$. The reactive power command $Q^*$ is obtained by adding the reactive power correction $Q_{se}$ to the instantaneous reactive power $Q_L$ for the PF correction. Accordingly, the $\alpha\beta$ axis control commands $i_{o\alpha}^*$ and $i_{o\beta}^*$ are computed as follows [19]:

$$\begin{bmatrix} i_{o\alpha}^* \\ i_{o\beta}^* \end{bmatrix} = \frac{1}{v_\alpha^2 + v_\beta^2} \begin{bmatrix} v_\alpha & -v_\beta \\ v_\beta & v_\alpha \end{bmatrix} \begin{bmatrix} P^* \\ Q^* \end{bmatrix} \tag{8}$$

The three-phase current commands $i_{oa}^*$, $i_{ob}^*$, $i_{oc}^*$ are obtained in accordance with the $\alpha\beta/abc$ coordinate transformation as follows:

$$\begin{bmatrix} i_{oa}^* \\ i_{ob}^* \\ i_{oc}^* \end{bmatrix} = \frac{2}{3} \begin{bmatrix} 1 & 0 \\ -\frac{1}{2} & -\frac{\sqrt{3}}{2} \\ -\frac{1}{2} & \frac{\sqrt{3}}{2} \end{bmatrix} \begin{bmatrix} i_{o\alpha}^* \\ i_{o\beta}^* \end{bmatrix} \tag{9}$$

Finally, the current commands $u_{comu}$, $u_{comv}$, $u_{comw}$ are computed for the SPWM switching signals.

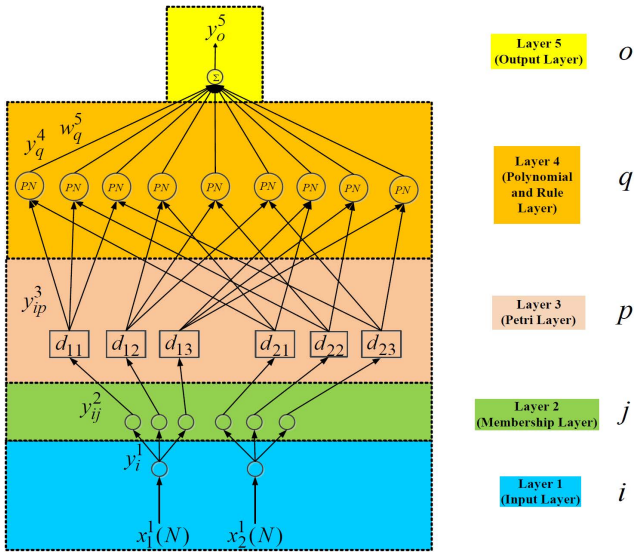


**FIGURE 4.** Network structure of proposed PPFNN.

## III. PROPOSED PPFNN CONTROLLER

On account of the uncomplicated structure and easy implementation, the PI controller is popularly utilized in different applications. Nevertheless, because the obtained parameters of the PI controller are only for the assumed situation, the function of the system using the conventional PI controller will be decreased in the case of the external interference and disturbance such as the sudden load variations. In other words, the PI controller can't cope with the system uncertainties such as the external disturbances and parameter variations. Furthermore, since the slow dynamic response and poor harmonic compensation capability of the traditional droop controls seriously deteriorate the power quality and system stability in the islanding microgrid [10], [11], an online trained PPFNN controller is firstly proposed as the DC-link voltage controller to supersede the conventional PI controller in the DSTATCOM. The proposed PPFNN controller comprises the input layer, membership layer, petri layer, polynomial and rule layer, and output layer. The network structure and online learning strategy of the proposed PPFNN is represented in Fig. 4 and derived in detail as follows:

### A. NETWORK STRUCTURE OF PPFNN

#### 1) INPUT LAYER

The input and output of this layer are depicted as:

$$net_i^1(N) = x_i^1(N) \tag{10}$$

$$y_i^1(N) = f_i^1(net_i^1(N)) = net_i^1(N)\ i = 1, 2 \tag{11}$$

where $N$ expresses the $N$th iteration; $x_1^1(\mathrm{N}) = e$; $x_2^1(\mathrm{N}) = \dot{e}$. In this study, the input variables of the proposed PPFNN controller are the DC-link voltage error $e = V_{dc}^*$- $V_{dc}$, and its derivative $\dot{e}$ for maintaining the constant DC-link voltage of the DSTATCOM.

#### 2) MEMBERSHIP LAYER

In each node of this layer, the membership function is performed by the Gaussian function to implement the fuzzification operation. The adopted Gaussian function for the $j$th node is represented as:

$$net_{ij}^2(N) = -\frac{(y_i^1 - m_{ij}^2)^2}{(\sigma_{ij}^2)^2} \tag{12}$$

$$y_{ij}^2(N) = f_{ij}^2(net_{ij}^2(N)) = \exp(net_{ij}^2(N)), j = 1,\ 2, 3 \tag{13}$$

where $\sigma_{ij}^2$ and $m_{ij}^2$ are the standard deviation and the mean of the Gaussian function respectively; $y_{ij}^2$(N) is the output of this layer.

#### 3) PETRI LAYER

In accordance with the PN theory, the competition law is utilized to select the suitable fired nodes for generating the tokens in the petri layer [4]. The PN is composed of two types of nodes: transition and place. When the token is created in input place, the transition is in enable state. Consequently, the condition of the fired or unfired transition can be described as:

$$t_{ip}^3(N) = \begin{cases} 1, \mathrm{y}_{ij}^2(N) \geq d_{ij} \\ 0, \mathrm{y}_{ij}^2(N) < d_{ij}, \end{cases} \quad p = 1, 2, 3 \tag{14}$$

$$d_{ij} = \frac{\alpha \exp(-\beta H)}{1 + \exp(-\beta H)} \tag{15}$$

where $\alpha$ and $\beta$ are positive constants and set to be 2 and 1.8 respectively by empirical rules; $t_{ip}^3$(N) is the transition; $d_{ij}$ is the dynamic threshold value and is varied by the function H in the following [2], [4]:

$$H = \frac{1}{2}(x_1^1(N) + x_2^1(N)) \tag{16}$$

When the transitions are fired, the required tokens are removed from its input places and new tokens are generated at each output place. On the other hand, when the transitions are unfired, the tokens will stay in original input place. Thereupon, the output and input of this layer are described as:

$$net_{ip}^3(N) = \begin{cases} y_{ij}^2(N), t_{ip}^3(N) = 1 \\ 0, t_{ip}^3(N) = 0 \end{cases} \tag{17}$$

$$y_{ip}^3(N) = f_{ip}^3(net_{ip}^3(N)) = net_{ip}^3(N) \tag{18}$$

#### 4) POLYNOMIAL AND RULE LAYER

The relationship of the input and output of the polynomial theory is denoted as follows [35], [36]:

$$net_q^4(N) = C_{q1}(y_{1p}^3 + y_{2p}^3) + C_{q2}(y_{1p}^3 y_{1p}^3 + y_{2p}^3 y_{2p}^3 + y_{1p}^3 y_{2p}^3) \tag{19}$$

$$y_q^4(N) = f_q^4(net_q^4(N)) = net_q^4(N),\ q = 1, \cdots, 9 \tag{20}$$

where $C_{q1}$ and $C_{q2}$ represent the coefficients, respectively; $y_q^4(N)$ is the estimated output of this layer.

#### 5) OUTPUT LAYER

In this layer, the defuzzification is implemented by using the summation operation $\sum$ and denoted in the following:

$$net_o^5(N) = \sum_{q=1}^{9} w_q^5 y_q^4(N), o = 1 \tag{21}$$

$$y_o^5(N) = f_o^5(net_o^5(N)) = net_o^5(N) \tag{22}$$

where $w_q^5$ is the connected weight between the output layer and the polynomial and rule layer; $y_o^5(N)$ is the output of the proposed PPFNN controller, which is equal to the power loss command $P_{loss}$ of the DSTATCOM as shown in Fig. 3 for maintaining the constant DC-link voltage during the load variations.

### B. ONLINE LEARNING STRATEGY

In accordance with the supervised gradient decent method, the proposed online trained PPFNN controller is to recursively acquire a gradient vector, which is the derivative of an error function with respect to the various parameters of the network. In this study, the error function $E(N)$ is represented as:

$$E(N) = \frac{1}{2}\left(V_{dc}^* - V_{dc}\right)^2 = \frac{1}{2}e^2 \tag{23}$$

The online learning strategy of the proposed PPFNN for DC-link voltage control is depicted in the following:

#### 1) OUTPUT LAYER

The error term to be propagated is acquired as:

$$\delta_o^5 = -\frac{\partial E}{\partial y_o^5(N)} = -\frac{\partial E}{\partial V_{dc}}\frac{\partial V_{dc}}{\partial y_o^5(N)} \tag{24}$$

By means of the chain rule, the connected weight can be updated by the amount:

$$\Delta w_q^5 = -\eta_1 \frac{\partial E}{\partial w_q^5} = -\eta_1 \frac{\partial E}{\partial y_o^5(N)}\frac{\partial y_o^7(N)}{\partial w_q^5} = \eta_1 \delta_o^5 y_q^4 \tag{25}$$

where $\eta_1$ is the learning rate. Afterward, the connected weight $\Delta w_q^5$ is updated and described as follows:

$$w_q^5(N+1) = w_q^5(N) + \Delta w_q^5 \tag{26}$$

#### 2) POLYNOMIAL AND RULE LAYER

The error term of this layer is derived as:

$$\delta_q^4 = -\frac{\partial E}{\partial y_q^4(N)} = -\left[\frac{\partial E}{\partial y_o^5(N)}\right]\frac{\partial y_o^5(N)}{\partial y_q^4} = \delta_o^5 w_q^5 \tag{27}$$

The updates of the coefficients $C_{q1}$ and $C_{q2}$ are computed by using the chain rule:

$$\Delta C_{q1} = -\eta_{q1}\frac{\partial E}{\partial C_{q1}(N)} = -\eta_{q2}\left[\frac{\partial E}{\partial y_o^2(N)}\frac{\partial y_o^2(N)}{\partial y_q^4}\right]\frac{\partial y_q^4}{\partial C_{q1}(N)}$$
$$= \eta_{q1}\delta_q^4\left(y_{1p}^3 + y_{2p}^3\right) \tag{28}$$

$$\Delta C_{q2} = -\eta_{q2}\frac{\partial E}{\partial C_{q2}(N)} = -\eta_{q2}\left[\frac{\partial E}{\partial y_o^2(N)}\frac{\partial y_o^2(N)}{\partial y_q^4}\right]\frac{\partial y_q^4}{\partial C_{q2}(N)}$$
$$= \eta_{q2}\delta_q^4\left(y_{1p}^3 y_{1p}^3 + y_{2p}^3 y_{2p}^3 + y_{1p}^3 y_{2p}^3\right) \quad (29)$$

where $\eta_{q1}$ and $\eta_{q2}$ are the learning rates. Thereupon, the coefficients $C_{q1}$ and $C_{q2}$ are updated in accordance with the following equations:

$$C_{q1}(N+1) = C_{q1}(N) + \Delta C_{q1} \quad (30)$$
$$C_{q2}(N+1) = C_{q2}(N) + \Delta C_{q2} \quad (31)$$

### 3) MEMBERSHIP LAYER

In membership layer, the error term to be calculated and propagated is given as:

$$\delta_{ij}^2 = -\frac{\partial E}{\partial net_{ij}^2(N)} = -\left[\frac{\partial E}{\partial y_o^5(N)}\frac{\partial y_o^5(N)}{\partial y_q^4}\right]\frac{\partial y_q^4(N)}{\partial y_{ij}^2(N)}\frac{\partial y_{ij}^2(N)}{\partial net_{ij}^2(N)}$$
$$= \sum_q \delta_q^4 y_{ij}^2\left[C_{q1} + C_{q2}\left(2y_{ij}^2 + y_{km}^2\right)\right]$$
$$k = \begin{cases} 2, i = 1 \\ 1, i = 2 \end{cases} ; m = \begin{cases} q - 3j + 3, i = 1 \\ \dfrac{q - j + 3}{3}, i = 2 \end{cases} \quad (32)$$

Furthermore, the updated amounts of the mean $\Delta m_{ij}^2$ and the standard deviation $\Delta\sigma_{ij}^2$ of the membership functions are computed respectively by means of the chain rule in the following:

$$\Delta m_{ij}^2 = -\eta_m\frac{\partial E}{\partial m_{ij}^2}$$
$$= -\eta_m\left[\frac{\partial E}{\partial y_o^5(N)}\frac{\partial y_o^5(N)}{\partial y_{ij}^2(N)}\frac{\partial y_{ij}^2(N)}{\partial net_{ij}^2(N)}\right]\frac{\partial net_{ij}^2(N)}{\partial m_{ij}^2(N)}$$
$$\eta_m\delta_{ij}^2\frac{2(y_i^1 - m_{ij}^2)}{(\sigma_{ij}^2)^2} \quad (33)$$
$$\Delta\sigma_{ij}^2 = -\eta_\sigma\frac{\partial E}{\partial\sigma_{ij}^2}$$
$$= -\eta_\sigma\left[\frac{\partial E}{\partial y_o^5(N)}\frac{\partial y_o^5(N)}{\partial y_{ij}^2(N)}\frac{\partial y_{ij}^2(N)}{\partial net_{ij}^2(N)}\right]\frac{\partial net_{ij}^2(N)}{\partial\sigma_{ij}^2(N)}$$
$$= \eta_\sigma\delta_{ij}^2\frac{2(y_i^1 - m_{ij}^2)^2}{(\sigma_{ij}^2)^3} \quad (34)$$

where $\eta_m$ and $\eta_\sigma$ are the learning rates of the mean and standard deviation respectively. Thus, the mean $m_{ij}^2$ and standard deviation $\sigma_{ij}^2$ of the membership functions are updated as:

$$m_{ij}^2(N+1) = m_{ij}^2(N) + \Delta m_{ij}^2 \quad (35)$$
$$\sigma_{ij}^2(N+1) = \sigma_{ij}^2(N) + \Delta\sigma_{ij}^2 \quad (36)$$

In consequence of the system uncertainties such as the parameter variations and external disturbances in the dynamic DSTATCOM, the exact calculation of the Jacobian of the DSTATCOM, $\partial V_{dc}/y_o^5(N)$, cannot be resolved. Accordingly, the delta adaptation law is utilized in the following to solve the above problem and to improve the online learning rate of the parameters in the proposed PPFNN [4].

$$\delta_o^5 \cong (V_{dc}^* - V_{dc}) + (\dot{V}_{dc}^* - \dot{V}_{dc}) = e + \dot{e} \quad (37)$$

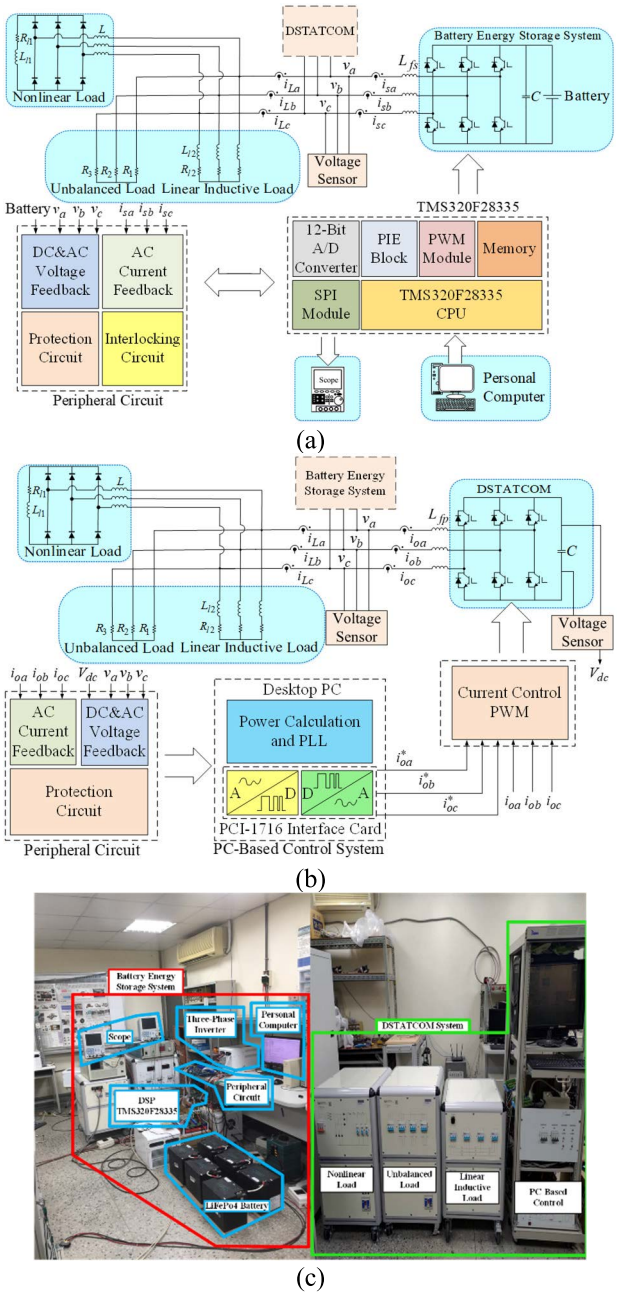


**FIGURE 5.** Droop controlled microgrid with DSTATCOM in islanding mode. (a) Block diagram of DSP-based storage system. (b) Block diagram of PC-based DSTATCOM. (c) Photo of experimental setup.

## IV. EXPERIMENTAL DESIGN AND RESULTS

In order to verify the effectiveness of the proposed PPFNN controller, the droop controlled microgrid with DSTATCOM operated in islanding mode is developed and illustrated in Fig. 5. The block diagram of the digital signal processor

**TABLE 1. Different nonlinear, linear inductive and three-phase unbalanced loads for droop controlled microgrid.**

| Load Condition | Nonlinear Load | Linear Inductive Load | Three-Phase Unbalanced Load |
|---|---|---|---|
| Load 1 | $L_{l1}$= 1 mH, $R_{l1}$= 100 Ω | $R_{l2}$= 25Ω, $L_{l2}$= 50 mH | $R_1$= 80Ω, $R_2$= 40Ω, $R_3$= 160Ω |
| Load 2 | $L_{l1}$= 1 mH, $R_{l1}$= 33 Ω | $R_{l2}$= 25Ω, $L_{l2}$= 50 mH | $R_1$= 80Ω, $R_2$= 40Ω, $R_3$= 160Ω |

(DSP)-based storage system is provided in Fig. 5(a). The control algorithms of the storage system, including the PLL, droop controls and the power calculation are carried out by the DSP TMS320F28335 with 1 ms sampling time and 16 kHz switching frequency. The block diagram of the personal computer (PC)-based DSTATCOM is illustrated in Fig. 5(b). The peripheral circuits of the DSTATCOM consist of the current, voltage and protection circuits. The control algorithm and the proposed PPFNN as the DC-link voltage controller for the DSTATCOM are implemented by the Matlab and Simulink software with 0.5 ms sampling time and 10 kHz switching frequency. The photo of the experimental setup is represented in Fig. 5(c). Moreover, the normal frequency and the line to line voltage of the droop controlled microgrid in islanding mode without load are set to be 60 Hz and 110 Vrms. The DC-link voltage command $V_{dc}^{*}$ of the DSTATCOM is set to be 190 V. Furthermore, in this study, since the storage system is a non-linear time-varying system, the parameters of the angular frequency and voltage controllers, namely PI controllers, used in the storage system are obtained by trial and error to achieve the exact tracking control of the frequency and voltage as shown in Fig. 2. The resulted parameters are $k_P = 1$, $k_I = 0.01$ for the angular frequency control and $k_P = 0.002$, $k_I = 0.001$ for the voltage control. In addition, the parameters of the PI controller in the DSTATCOM for the DC-link voltage control as shown in Fig. 3 are also obtained by trial and error to achieve good transient and steady-state control performance. The obtained parameters are $k_P = 5$, $k_I = 0.1$ for the DC-link voltage control. Additionally, the different nonlinear, linear inductive and the three-phase unbalanced loads cause the deteriorated power quality are designed in Table 1. The nonlinear load is designed to cause the high current THD. The linear inductive load leads to the lagging PF. The designed three-phase unbalanced load results in the three-phase unbalanced currents. Moreover, to demonstrate the compensation performance of the three-phase unbalanced system currents, the unbalanced current ratio *CUR* is designed in the following.

$$CUR = \frac{\text{Max.}(i_{sa}, i_{sb}, i_{sc}) - \text{Min.}(i_{sa}, i_{sb}, i_{sc})}{\text{Avg.}(i_{sa}, i_{sb}, i_{sc})} \times 100\% \tag{38}$$

where $\text{Min.}(i_{sa}, i_{sb}, i_{sc})$ and $\text{Max.}(i_{sa}, i_{sb}, i_{sc})$ represent the minimum and the maximum currents of the output currents $i_{sa}, i_{sb}, i_{sc}$ respectively; $\text{Avg.}(i_{sa}, i_{sb}, i_{sc})$ depicts the average current of the output currents $i_{sa}, i_{sb}, i_{sc}$. The lesser value the unbalanced current ratio *CUR* is, the better compensation performance the DSTATCOM possesses. In addition, according to the IEEE 519 regulation, the allowable current THD for power system is below 5% [38]. In order to verify the effectiveness of the DSTATCOM using the proposed PPFNN controller in the droop controlled microgrid for the improvements of the power quality and stability, two test cases are designed as follows: (1) Case 1: The droop controlled microgrid is equipped with load 1 as shown in Table 1, including the nonlinear, linear inductive and the three-phase unbalanced loads; (2) Case 2: The load is changed from load 1 to load 2. Additionally, the performance of the DSTATCOM using the conventional PI and FNN controllers as shown in Fig. 3 are also provided for comparison.

Firstly, the experimental result of the droop controlled microgrid without using the DSTATCOM for power quality improvement at case 1 is provided in Fig. 6. The responses of the system voltage $v_a$, output currents $i_{sa}, i_{sb}, i_{sc}$ of the storage system, load currents $i_{La}$, $i_{Lb}$, $i_{Lc}$ and the compensation current $i_{oa}$ of DSTATCOM are represented in Fig. 6(a). The responses of the active power $P_s$ of the storage system and the frequency $f_m$ of the microgrid are provided in Fig. 6(b). The responses of the reactive power $Q_s$ of the storage system and the peak value of the phase voltage $V_{an,peak}$ of the microgrid are presented in Fig. 6(c). According to the experimental results as shown in Fig. 6(a), since the absence of the DSTATCOM in the droop controlled microgrid, the different nonlinear, linear inductive and the three-phase unbalanced loads seriously deteriorate the power quality. The current THD and lagging PF are 8.35 % and 0.93. The waveforms of the currents $i_{sa}, i_{sb}, i_{sc}$ aren't sinusoidal and unbalanced resulted from the three-phase unbalanced loads. The unbalanced current ratio *CUR* is 12 %. Moreover, due to the $P$-$\omega$ and $Q$-$V$ droop characteristics, the droop controls reduce the frequency $f_m$ and the phase voltage $V_{an,peak}$ of the microgrid to dispatch the active and reactive powers of the storage system according to the loads. The frequency $f_m$ and the phase voltage $V_{an,peak}$ of the microgrid are self-regulated to be 59.82 Hz and 80.5 V for dispatching the active power 498 W and reactive power 186 Var as shown in Figs. 6(b) and 6(c). Moreover, the experimental result of the droop controlled microgrid using the PI-based DSTATCOM for power quality improvements at case 1 is provided in Fig. 7. The responses of the system voltage $v_a$, output currents $i_{sa}, i_{sb}, i_{sc}$ of the storage system, load currents $i_{La}$, $i_{Lb}$, $i_{Lc}$ and the compensation current $i_{oa}$ of the DSTATCOM are given in Fig. 7(a). The responses of the active power $P_s$ of the storage system and the frequency $f_m$ of the microgrid are provided in Fig. 7(b). The responses of the reactive power $Q_s$ of the storage system and the peak value of the phase voltage $V_{an,peak}$ of the microgrid are presented in Fig. 7(c). The response of the DC-link voltage of the DSTATCOM is given in Fig. 7(d). From the experimental result, since the PI-based DSTATCOM is adopted in the droop controlled microgrid, the power quality improvements can be achieved as shown in Figs. 7(a) and 7(c). The current THD and lagging

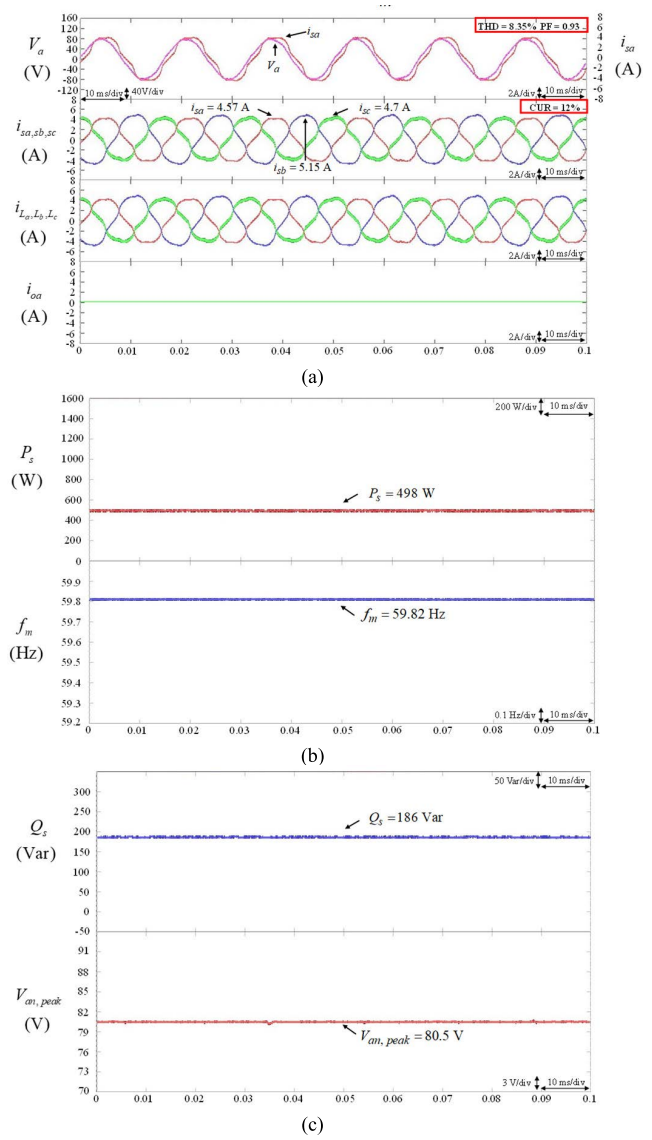


**FIGURE 6.** Experimental results of droop controlled microgrid without using DSTATCOM at case 1. (a) Responses of system voltage, output currents of storage system, load currents and compensation current of DSTATCOM. (b) Responses of active power of storage system and frequency of microgrid. (c) Responses of reactive power of storage system and peak value of phase voltage of microgrid.

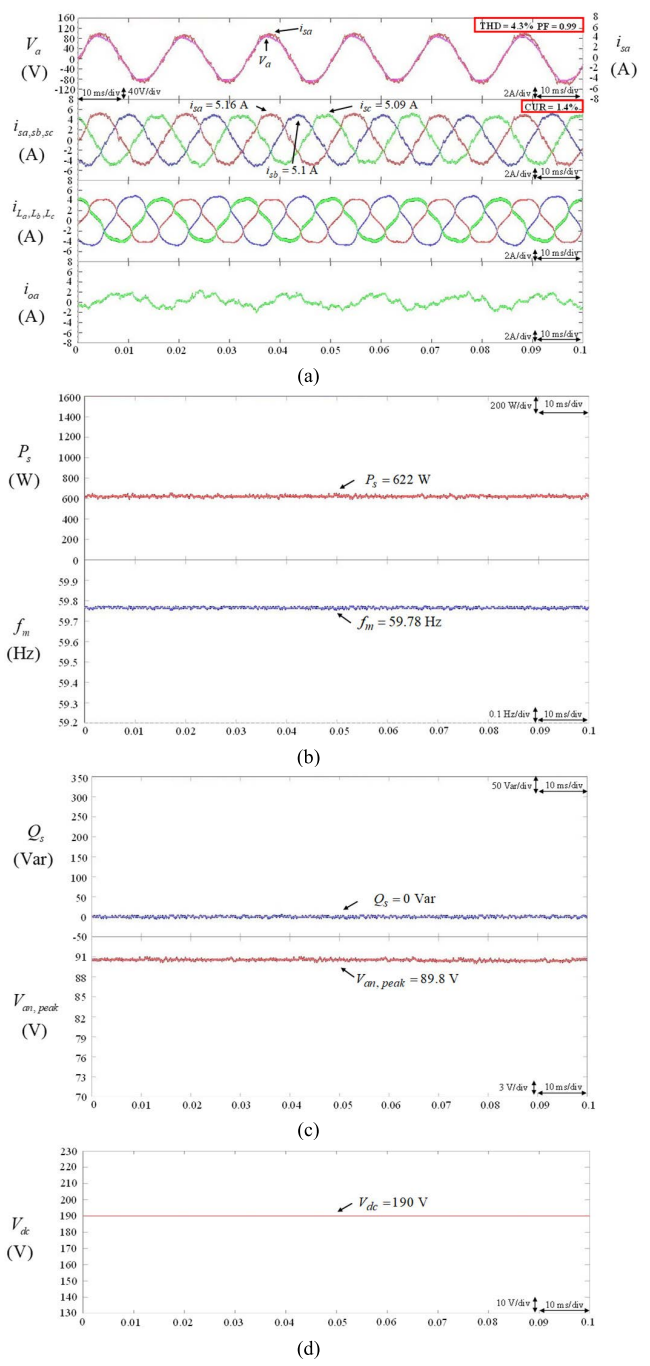


**FIGURE 7.** Experimental results of droop controlled microgrid using PI-based DSTATCOM at case 1. (a) Responses of system voltage, output currents of storage system, load currents and compensation current of DSTATCOM. (b) Responses of active power of storage system and frequency of microgrid. (c) Responses of reactive power of storage system and peak value of phase voltage of microgrid. (d) Response of DC-link voltage of DSTATCOM.

PF of the microgrid have been improved to be 4.3 % and 0.99. The waveforms of the currents $i_{sa}, i_{sb}, i_{sc}$ have been compensated to be sinusoidal and balanced. The unbalanced current ratio *CUR* is reduced to be 1.4 %. Furthermore, the PI-based DSTATCOM also compensates the reactive power for the voltage support in the droop controlled microgrid. Hence, the peak value of the phase voltage $V_{an,peak}$ of the microgrid has been returned to the normal value 89.8 V and the reactive power $Q_s$ of the storage system reduces to be 0 Var in accordance with the $Q$-$V$ droop characteristic as shown in Fig. 7(c). In addition, the experimental result of the droop controlled microgrid using the FNN-based DSTATCOM at case 1 is represented in Fig. 8. According to the experimental results, the power quality has been improved. The current THD and lagging PF of the microgrid system are 3.8 % and 0.99. The unbalanced current ratio *CUR* is 1.3 %. On the other hand, the experimental result of the droop controlled microgrid using the proposed PPFNN-based

**TABLE 2. Current THD, PF and CUR of DSTATCOM using PI, FNN and proposed PPFNN controllers at case 1.**

| Case Condition | DC-Link Voltage Controller | Current THD | PF | CUR |
|---|---|---|---|---|
| Case 1 | Without DSTATCOM | 8.35 % | 0.93 | 12 % |
| | PI | 4.3 % | 0.99 | 1.4 % |
| | FNN | 3.8 % | 0.99 | 1.3 % |
| | PPFNN | 3 % | 0.99 | 1 % |

DSTATCOM at case 1 is provided in Fig. 9. In accordance with the experimental results, since the proposed PPFNN controller combines the advantages of the FNN, PN and PNN, comparing to the experimental results of the DSTATCOM using the PI and FNN DC-link voltage controllers, the power quality of the droop controlled microgrid is much improved as shown in Fig. 9(a). The current THD and PF of the microgrid are 3 % and 0.99. The unbalanced current ratio *CUR* is 1 %. In other words, the proposed PPFNN-based DSTATCOM can effectively overcome the drawback of the droop controls, such as the poor harmonic compensation capability [10], [11]. Additionally, the current THD, PF and CUR of the DSTATCOM using the PI, FNN and the proposed PPFNN controllers at case 1 are provided in Table 2. According to the experimental results shown in Figs. 6-9 and Table 2, the deteriorated power quality resulted from the nonlinear, linear inductive and the three-phase unbalanced loads, and the voltage support have been much improved by the proposed PPFNN controller.

Finally, to verify the performance of the DSTATCOM under load variation, the droop controlled microgrid operated at case 2 is demonstrated. At this case, the load is changed from load 1 to load 2 at 1.5 s. The experimental result of the droop controlled microgrid using the PI-based DSTATCOM at case 2 is represented in Fig. 10. The responses of the active power $P_s$ of the storage system and the frequency $f_m$ of the microgrid are provided in Fig. 10(a). The responses of the reactive power $Q_s$ of the storage system and the peak value of the phase voltage $V_{an,peak}$ of the microgrid are presented in Fig. 10(b). The responses of the DC-link voltage of the DSTATCOM and the output current $i_{sa}$ of the storage system are given in Fig. 10(c). According to the experimental results as shown in Fig. 10 (a), the $P$-$\omega$ droop control reduces the frequency $f_m$ of the microgrid to dispatch the output active power of the storage system according to the varying loads. The frequency $f_m$ of the microgrid is self-regulated from 59.78 Hz to 59.66 Hz at 1.5 s. The active power $P_s$ of the storage system is changed from 622 W to 1000 W at 1.5 s. Moreover, since the PI-based DSTATCOM is utilized in the droop controlled microgrid, the reactive power compensation for the voltage support can be achieved as shown in Fig. 10(b). The reactive power $Q_s$ of the storage system and the peak value of the phase voltage $V_{an,peak}$ of the microgrid are 0 Var and 89.8 V, respectively. However, the response of the DC-link voltage of

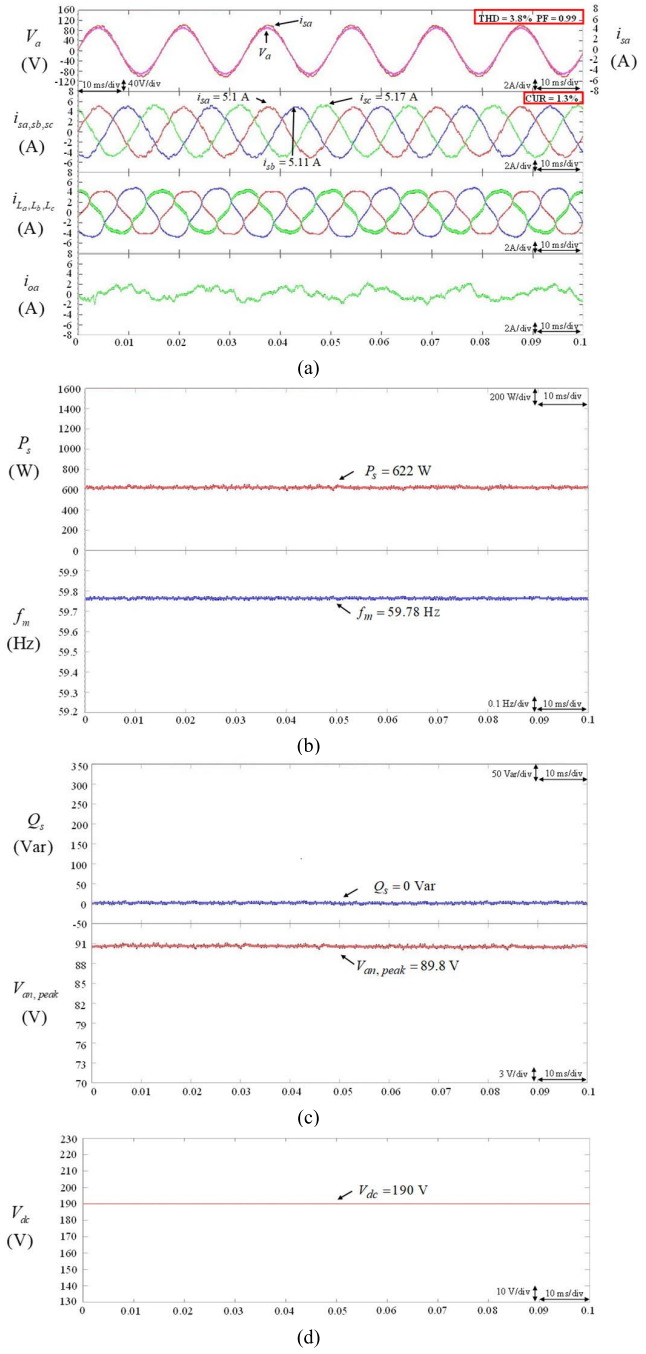


**FIGURE 8. Experimental results of droop controlled microgrid using FNN-based DSTATCOM at case 1. (a) Responses of system voltage, output currents of storage system, load currents and compensation current of DSTATCOM. (b) Responses of active power of storage system and frequency of microgrid. (c) Responses of reactive power of storage system and peak value of phase voltage of microgrid. (d) Response of DC-link voltage of DSTATCOM.**

the DSTATCOM fluctuates at the moment of the load change due to the poor robust control property of the PI controller as show in Fig. 10(c), which causes the seriously fluctuated phase voltage $V_{an,peak}$ of the microgrid and the reactive power $Q_s$ of the storage system at 1.5 s as shown in Figs. 10(b). On account of the fluctuated voltage of the microgrid, the

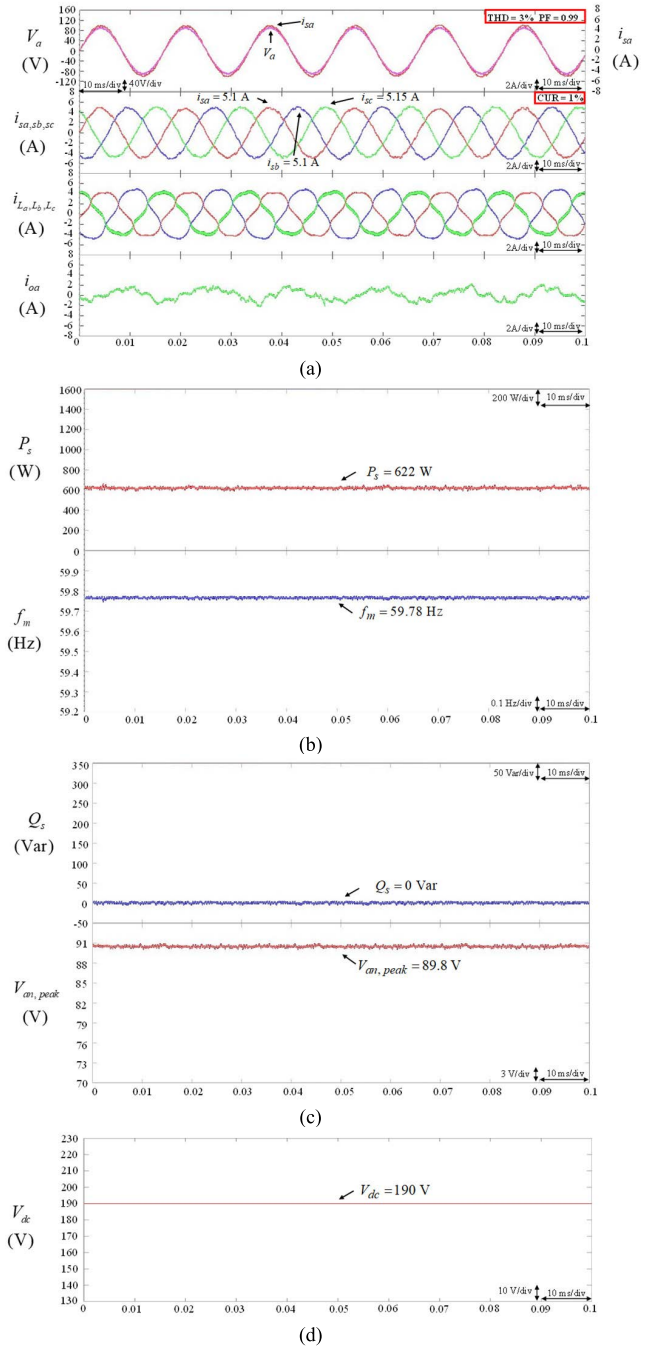


**FIGURE 9.** Experimental results of droop controlled microgrid using proposed PPFNN-based DSTATCOM at case 1. (a) Responses of system voltage, output currents of storage system, load currents and compensation current of DSTATCOM. (b) Responses of active power of storage system and frequency of microgrid. (c) Responses of reactive power of storage system and peak value of phase voltage of microgrid. (d) Response of DC-link voltage of DSTATCOM.

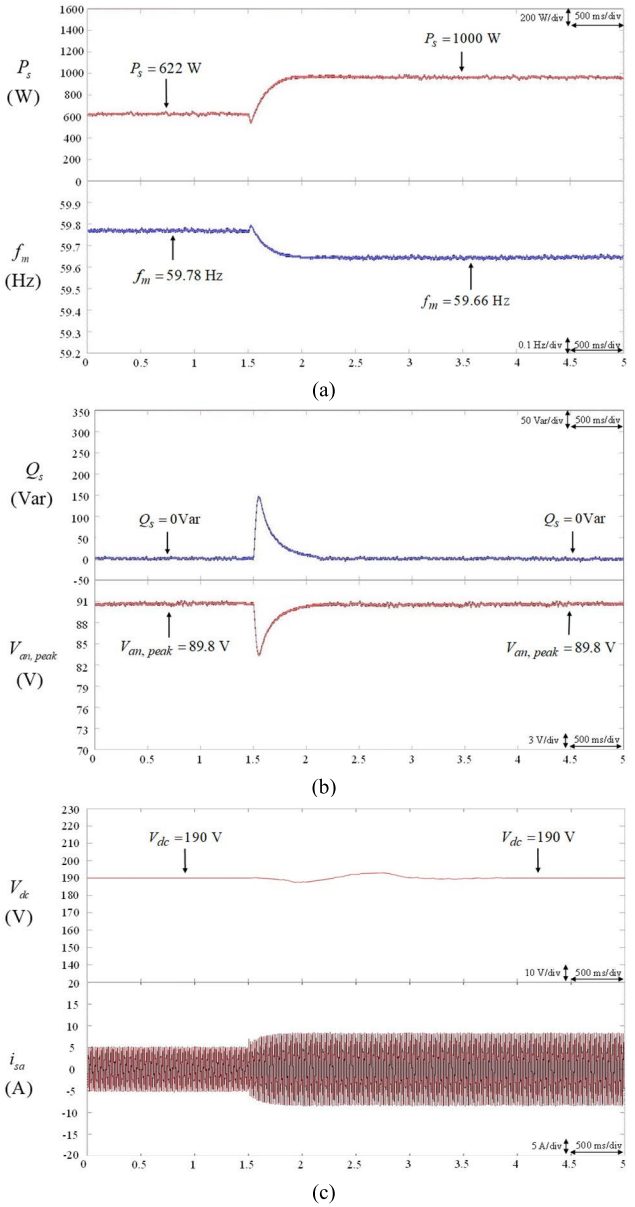


**FIGURE 10.** Experimental results of droop controlled microgrid using PI-based DSTATCOM at case 2. (a) Responses of active power of storage system and frequency of microgrid. (b) Responses of reactive power of storage system and peak value of phase voltage of microgrid. (c) Responses of DC-link voltage of DSTATCOM and output current of storage system.

responses of the frequency $f_m$ and the active power $P_s$ are also slow and degraded under load variation. Hence, owing to the disadvantages of the PI controller, the transient responses of the DC-link voltage of the DSTATCOM, the power outputs of the storage system and the frequency and the voltage of the microgrid are very sluggish during the load change. Furthermore, the experimental result of the droop controlled microgrid using the FNN-based DSTATCOM at case 2 is illustrated in Fig. 11. From the experimental result as shown in Fig. 11(c), since the transient response of the DC-link voltage of the DSTATCOM is improved at the moment of the load change, the responses of the power outputs of the storage system and the frequency and the voltage of the microgrid are also improved during the load change as shown in Figs. 11(a) and 11(b). On the other hand, the experimental result of the droop controlled microgrid using the proposed PPFNN-based

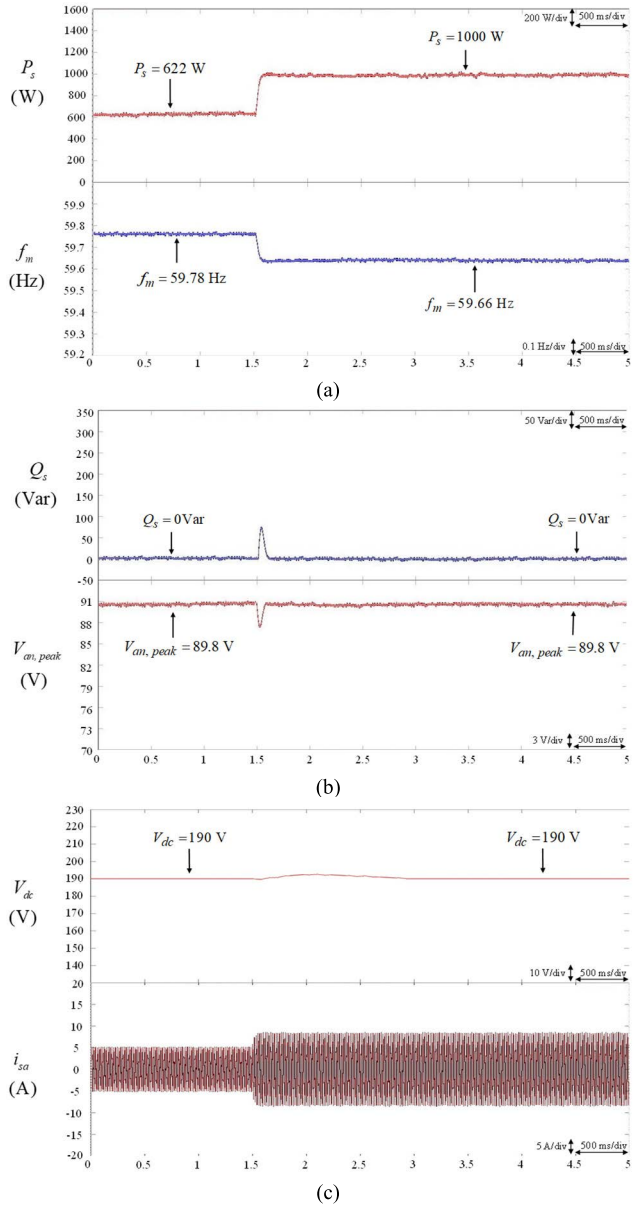


**FIGURE 11.** Experimental results of droop controlled microgrid using FNN-based DSTATCOM at case 2. (a) Responses of active power of storage system and frequency of microgrid. (b) Responses of reactive power of storage system and peak value of phase voltage of microgrid. (c) Responses of DC-link voltage of DSTATCOM and output current of storage system.

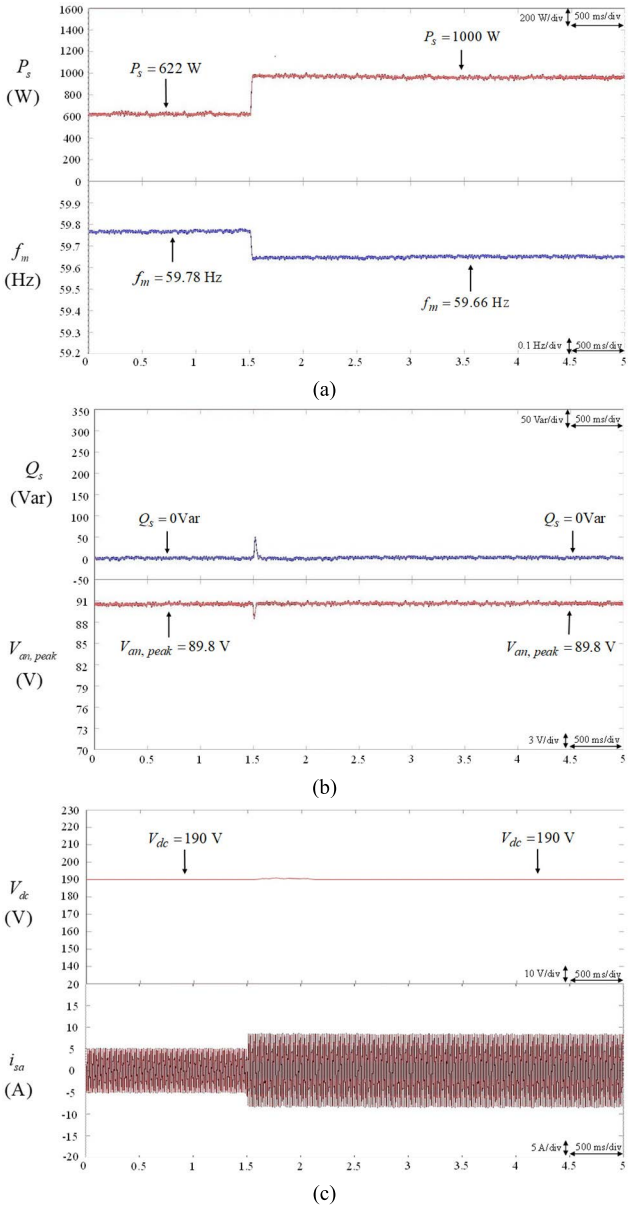


**FIGURE 12.** Experimental results of droop controlled microgrid using proposed PPFNN-based DSTATCOM at case 2. (a) Responses of active power of storage system and frequency of microgrid. (b) Responses of reactive power of storage system and peak value of phase voltage of microgrid. (c) Responses of DC-link voltage of DSTATCOM and output current of storage system.

DSTATCOM at case 2 is represented in Fig. 12. In accordance with the experimental results as shown in Fig. 12(c), the transient response of the DC-link voltage of the DSTATCOM is much improved at 1.5 s due to the powerful ability of the proposed PPFNN. In other words, the DC-link voltage of the DSTATCOM can maintain the constant voltage effectively during the load variation. Hence, the transient responses of the power outputs of the storage system and the frequency and the voltage of the microgrid are also much improved and fast comparing with the PI and FNN-based DSTATCOM. In addition, the active power error, reactive power error, frequency error, voltage error and the transient time of the droop controlled microgrid with DSTATCOM using the PI, FNN and the proposed PPFNN controllers at case 2 are provided in Tables 3 and 4. The overshoot and undershoot of the DC-link voltage and the DC-link voltage transient time of the DSTATCOM using the PI, FNN and the proposed PPFNN controllers at case 2 are given in Table 5. According to the experimental results as shown in Figs. 10-12 and Tables 3-5, the DSTATCOM using the proposed PPFNN controller can effectively maintain the DC-link voltage and enhance the power quality improvements under load variation. Therefore,

**TABLE 3.** Active power error, frequency error and transient time of droop controlled microgrid with DSTATCOM using PI, FNN and proposed PPFNN controllers at case 2.

| Case Condition | Controller | Active Power Error | Frequency Error | Transient Time |
|---|---|---|---|---|
| Case 2 | PI | 88 W | 0.031 Hz | 1185 ms |
| | FNN | 4 W | 0.0014 Hz | 300 ms |
| | PPFNN | 0.5 W | 0.00017 Hz | 110 ms |

**TABLE 4.** Reactive power error, voltage error and transient time of droop controlled microgrid with DSTATCOM using PI, FNN and proposed PPFNN controllers at case 2.

| Case Condition | Controller | Reactive Power Error | Peak of a-Phase Voltage Error | Transient Time |
|---|---|---|---|---|
| Case 2 | PI | 142 VAR | 7.1 V | 885 ms |
| | FNN | 80.5 VAR | 4.02 V | 205 ms |
| | PPFNN | 42 VAR | 2.1 V | 100 ms |

**TABLE 5.** Overshoot and undershoot of DC-Link voltage and DC-Link voltage transient time of DSTATCOM using PI, FNN and proposed PPFNN controllers at case 2.

| Case Condition | Controller | DC Link Voltage Error | | DC Link Voltage Transient Time |
|---|---|---|---|---|
| | | Overshoot | Undershoot | |
| Case 2 | PI | 3 V | 2.8 V | 2450 ms |
| | FNN | 3 V | 0 V | 1400 ms |
| | PPFNN | 1 V | 0 V | 550 ms |

the power quality and the stability of the droop controlled microgrid under load variation can be guaranteed and the drawback of the droop controls, such as the slow dynamic response, can be overcome by the proposed PPFNN based DSTATCOM.

## V. CONCLUSION

On account of the $Q$-$V$ droop characteristic and the existence of the various loads, the power quality problems are very serious in the droop controlled microgrid. Moreover, the unsuitable design of the DC-link voltage control of the DSTATCOM results in the degenerated performance of the power quality improvements under load variation. Hence, to effectively improve the power quality of the droop controlled microgrid and the transient response of the DC-link voltage of the DSTATCOM under load variation, an online trained PPFNN controller is proposed as the DC-link voltage controller to supersede the conventional PI controller. Furthermore, the effectiveness of the droop controlled microgrid using the proposed PPFNN-based DSTATCOM is verified by the experimental results. Comparing to the experimental results of the DSTATCOM using the PI and FNN controllers, the DSTATCOM using the proposed PPFNN controller can effectively maintain the DC-link voltage, enhance the power quality improvement and increase the system stability under load variation due to the powerful ability of the proposed PPFNN.

The major contributions of this study are: (i) the successful developments of the droop controlled microgrid and the IRP theory based-DSTATCOM; (ii) the successful development of the proposed PPFNN controller; (iii) the successful integration of the droop controlled microgrid and the proposed PPFNN-based DSTATCOM to improve the power quality, including the unbalanced current compensation, the current THD reduction, the reactive power compensation for the voltage support and PF correction; (iv) the successful implementation of the proposed PPFNN-based DSTATCOM to maintain the constant DC-link voltage and to improve the system stability under load variation.

## ACKNOWLEDGMENT

The authors would like to thank Prof. Faa-Jeng Lin for his insightful comments regarding this work and the equipment support from Electric Machinery and Control Laboratory, National Central University, Taiwan.

## REFERENCES

[1] A. C. Moreira, H. K. M. Paredes, W. A. de Souza, F. P. Marafao, and L. C. P. da Silva, "Intelligent expert system for power quality improvement under distorted and unbalanced conditions in three-phase AC microgrids," *IEEE Trans. Smart Grid*, vol. 9, no. 6, pp. 6951–6960, Nov. 2018.

[2] K.-H. Tan, F.-J. Lin, C.-M. Shih, and C.-N. Kuo, "Intelligent control of microgrid with virtual inertia using recurrent probabilistic wavelet fuzzy neural network," *IEEE Trans. Power Electron.*, vol. 35, no. 7, pp. 7451–7464, Jul. 2020.

[3] K.-H. Tan and T.-Y. Tseng, "Seamless switching and grid reconnection of microgrid using Petri recurrent wavelet fuzzy neural network," *IEEE Trans. Power Electron.*, vol. 36, no. 10, pp. 11847–11861, Oct. 2021.

[4] F.-J. Lin, K.-H. Tan, C.-F. Chang, M.-Y. Li, and T.-Y. Tseng, "Development of intelligent controlled microgrid for power sharing and load shedding," *IEEE Trans. Power Electron.*, vol. 37, no. 7, pp. 7928–7940, Jul. 2022.

[5] R. Majumder, "Reactive power compensation in single-phase operation of microgrid," *IEEE Trans. Ind. Electron.*, vol. 60, no. 4, pp. 1403–1416, Apr. 2013.

[6] H. Shi, F. Zhuo, H. Yi, F. Wang, D. Zhang, and Z. Geng, "A novel real-time voltage and frequency compensation strategy for photovoltaic-based microgrid," *IEEE Trans. Ind. Electron.*, vol. 62, no. 6, pp. 4477–4487, Jun. 2015.

[7] M. Amir, A. K. Prajapati, and S. S. Refaat, "Dynamic performance evaluation of grid-connected hybrid renewable energy-based power generation for stability and power quality enhancement in smart grid," *Frontiers Energy Res.*, vol. 10, pp. 1–16, Mar. 2022.

[8] K. Singh, M. Amir, F. Ahmad, and S. S. Refaat, "Enhancement of frequency control for stand-alone multi-microgrids," *IEEE Access*, vol. 9, pp. 79128–79142, 2021.

[9] Zaheeruddin, K. Singh, and M. Amir, "Intelligent fuzzy TIDF-II controller for load frequency control in hybrid energy system," *IETE Tech. Rev.*, vol. 7, pp. 1–17, Nov. 2021.

[10] L. Wang, M.-C. Wong, X. Zhou, Z. He, Q. Xu, and L. Zhou, "A selective power droop control for hybrid interlinking converter in AC/LVDC microgrid," *IEEE Trans. Ind. Electron.*, vol. 68, no. 10, pp. 9046–9057, Oct. 2021.

[11] L. Wang, C.-S. Lam, and M.-C. Wong, "Multifunctional hybrid structure of SVC and capacitive grid-connected inverter (SVC//CGCI) for active power injection and nonactive power compensation," *IEEE Trans. Ind. Electron.*, vol. 66, no. 3, pp. 1660–1670, Mar. 2019.

[12] M. Bagheri, V. Nurmanova, O. Abedinia, and M. S. Naderi, "Enhancing power quality in microgrids with a new online control strategy for DSTATCOM using reinforcement learning algorithm," *IEEE Access*, vol. 6, pp. 38956–38996, 2018.

[13] H. K. Nguyen, H. Mohsenian-Rad, A. Khodaei, and Z. Han, "Decentralized reactive power compensation using Nash bargaining solution," *IEEE Trans. Smart Grid*, vol. 8, no. 4, pp. 1679–1688, Jul. 2017.
[14] L. Meng, X. Zhao, F. Tang, M. Savaghebi, T. Dragicevic, J. C. Vasquez, and J. M. Guerrero, "Distributed voltage unbalance compensation in islanded microgrids by using a dynamic consensus algorithm," *IEEE Trans. Power Electron.*, vol. 31, no. 1, pp. 827–838, Jan. 2016.
[15] M. Srinivas, I. Hussain, and B. Singh, "Combined LMS–LMF-based control algorithm of DSTATCOM for power quality enhancement in distribution system," *IEEE Trans. Ind. Electron.*, vol. 63, no. 7, pp. 4160–4168, Jul. 2016.
[16] H. Chen, A. Prasai, and D. Divan, "A modular isolated topology for instantaneous reactive power compensation," *IEEE Trans. Power Electron.*, vol. 33, no. 2, pp. 975–986, Feb. 2018.
[17] S. K. Patel, S. R. Arya, and R. Maurya, "Nonlinear adaptive Volterra filter for control of distribution static compensator," *IEEE J. Emerg. Sel. Topics Power Electron.*, vol. 5, no. 1, pp. 559–567, Mar. 2017.
[18] S. K. Patel, S. R. Arya, R. Maurya, and B. C. Babu, "Control scheme for DSTATCOM based on frequency-adaptive disturbance observer," *IEEE J. Emerg. Sel. Topics Power Electron.*, vol. 6, no. 3, pp. 1345–1354, Sep. 2018.
[19] B. Singh and J. Solanki, "A comparison of control algorithms for DSTATCOM," *IEEE Trans. Ind. Electron.*, vol. 56, no. 7, pp. 2738–2745, Jul. 2009.
[20] K. H. Tan, F. J. Lin, C. Y. Tsai, and Y. R. Chang, "A distribution static compensator using a CFNN-AMF controller for power quality improvement and DC-link voltage regulation," *Energies*, vol. 11, no. 8, pp. 1–17, 2018.
[21] J. Qi, W. Zhao, and X. Bian, "Comparative study of SVC and STATCOM reactive power compensation for prosumer microgrids with DFIG-based wind farm integration," *IEEE Access*, vol. 8, pp. 209878–209885, 2020.
[22] B. Singh, P. Jayaprakash, and D. P. Kothari, "A T-connected transformer and three-leg VSC based DSTATCOM for power quality improvement," *IEEE Trans. Power Electron.*, vol. 23, no. 6, pp. 2710–2718, Nov. 2008.
[23] A. Khoshooei, J. S. Moghani, I. Candela, and P. Rodriguez, "Control of D-STATCOM during unbalanced grid faults based on DC voltage oscillations and peak current limitations," *IEEE Trans. Ind. Appl.*, vol. 54, no. 2, pp. 1680–1690, Mar. 2018.
[24] K. K. Prasad, H. Myneni, and G. S. Kumar, "Power quality improvement and PV power injection by DSTATCOM with variable DC link voltage control from RSC-MLC," *IEEE Trans. Sustain. Energy*, vol. 10, no. 2, pp. 876–885, Apr. 2019.
[25] A. Salimi-Badr and M. M. Ebadzadeh, "A novel self-organizing fuzzy neural network to learn and mimic habitual sequential tasks," *IEEE Trans. Cybern.*, vol. 52, no. 1, pp. 323–332, Jan. 2022.
[26] Z. Zhang and Z. Yan, "An adaptive fuzzy recurrent neural network for solving the nonrepetitive motion problem of redundant robot manipulators," *IEEE Trans. Fuzzy Syst.*, vol. 28, no. 4, pp. 684–691, Apr. 2020.
[27] J. Zhuo, C. An, and J. Fei, "Fuzzy multiple hidden layer neural sliding mode control of active power filter with multiple feedback loop," *IEEE Access*, vol. 9, pp. 114294–114307, 2021.
[28] L. Liu, J. Fei, and C. An, "Adaptive sliding mode long short-term memory fuzzy neural control for harmonic suppression," *IEEE Access*, vol. 9, pp. 69724–69734, 2021.
[29] B. Cao, J. Zhao, Z. Lv, Y. Gu, P. Yang, and S. K. Halgamuge, "Multiobjective evolution of fuzzy rough neural network via distributed parallelism for stock prediction," *IEEE Trans. Fuzzy Syst.*, vol. 28, no. 5, pp. 939–952, Feb. 2020.
[30] K. H. Tan, F. J. Lin, and J. H. Chen, "A three-phase four-leg inverter-based active power filter for unbalanced current compensation using a Petri probabilistic fuzzy neural network," *Energies*, vol. 10, no. 12, pp. 1–21, 2017.
[31] R. Davidrajuh, "Extracting Petri modules from large and legacy Petri net models," *IEEE Access*, vol. 8, pp. 156539–156556, 2020.
[32] L. Rui, X. Chen, X. Wang, Z. Gao, X. Qiu, and S. Wang, "Multiservice reliability evaluation algorithm considering network congestion and regional failure based on Petri net," *IEEE Trans. Services Comput.*, vol. 15, no. 2, pp. 684–697, Mar. 2022.
[33] E. A. Alzalab, A. M. El-Sherbeeny, M. A. El-Meligy, and H. T. Rauf, "Trust-based Petri net model for fault detection and treatment in automated manufacturing systems," *IEEE Access*, vol. 9, pp. 157997–158009, 2021.
[34] A. G. Ivakhnenko, "Polynomial theory of complex systems," *IEEE Trans. Syst., Man, Cybern.*, vol. SMC-1, no. 4, pp. 364–378, Oct. 1971.
[35] W. Huang, S.-K. Oh, and W. Pedrycz, "Fuzzy wavelet polynomial neural networks: Analysis and design," *IEEE Trans. Fuzzy Syst.*, vol. 25, no. 5, pp. 1329–1341, Oct. 2017.
[36] S.-K. Oh, W. Pedrycz, and B.-J. Park, "Polynomial neural networks architecture: Analysis and design," *Comput. Elect. Eng.*, vol. 29, no. 6, pp. 703–725, 2003.
[37] B. Lei, X. Liu, S. Liang, W. Hang, Q. Wang, K. S. Choi, and J. Qin, "Walking imagery evaluation in brain computer interfaces via a multi-view multi-level deep polynomial network," *IEEE Trans. Neural Syst. Rehabil. Eng.*, vol. 27, no. 3, pp. 497–506, Mar. 2019.
[38] *IEEE Recommended Practice and Requirements for Harmonic Control in Electric Power Systems*, Standard 519-2014, 2014.

**KUANG-HSIUNG TAN** (Member, IEEE) received the B.S., M.S., and Ph.D. degrees in electrical and electronic engineering from the Chung Cheng Institute of Technology (CCIT), National Defense University, Taiwan, in 2002, 2007, and 2013, respectively. He has been a Faculty Member at CCIT, where he is currently an Associate Professor with the Department of Electrical and Electronic Engineering. His teaching and research interests include power electronics, power quality, microgrid systems, and intelligent control.

**MENG-YANG LI** received the B.S. degree in electronic engineering from the National Ilan University, Yilan County, Taiwan, in 2020, and the M.S. degree in electrical engineering from the National Central University, Chungli, Taiwan, in 2022. His research interests include power electronics, intelligent control, and microgrid systems.

**XIANG-YU WENG** was born in Hsinchu, Taiwan, in 1999. He received the B.S. degree in electrical engineering from the National United University, Miaoli City, Taiwan, in 2021. He is currently pursuing the M.S. degree with the National Central University, Chungli, Taiwan. His research interests include intelligent control and microgrid.